Effect of surfactants on drop formation flow patterns in a flow-focusing microchannel

*Maria Kalli, Panagiota Angeli**

ThAMeS Multiphase, Department of Chemical Engineering, University College London,

Torrington Place, London, WC1E 7JE, UK

*corresponding author: p.angeli@ucl.ac.uk

Abstract

The formation of droplets in an immiscible liquid in the presence of different surfactants was studied experimentally using a flow-focusing microchannel. A low viscosity silicone oil (4.6 mPa s) was used as the continuous phase and a mixture of 48% w/w water and 52% w/w glycerol was the dispersed phase. A cationic (CMC_{DTAB} = 20mM), an anionic (CMC_{SDS} = 11mM), and a non-ionic (CMC_{TX100} = 3.5mM) surfactant were added in the aqueous phase, at several concentrations. Five patterns of drop formation were identified, namely squeezing, dripping, jetting, threading and tip streaming/jetting, whose boundaries were affected by the surfactant type and concentration. Using dynamic interfacial tension values, it was possible to plot a universal flow pattern map with the capillary numbers of the two phases as coordinates, where the transition boundaries between the dripping and the jetting patterns collapsed for all fluid systems considered, including the solutions with and without surfactants.

Keywords: drop formation pattern maps, flow pattern transitions, surfactants, dynamic interfacial tension, capillary number, flow-focusing microchannel

1. INTRODUCTION

Microfluidic channels are widely used to produce droplets with controlled size, important in applications such as emulsification, inkjet printing and chemical analysis. Surface active agents such as surfactants are often added to vary interfacial properties and control drop size. Their versality allows surfactants to be used in a wide variety of products such as ink formulations, pharmaceuticals, cosmetics, motor oils, laundry detergents and household cleaning products. Recently, surfactants have been added in ink formulations for bioprinting of implantable organs (Murphy and Atala, 2014; Roth et al., 2004).

When two immiscible liquids join to form drops in microchannels different patterns can appear. Common patterns of drop formation include squeezing, dripping, jetting, threading and tip streaming (Lei et al., 2021). Jetting is widely used in inkjet printing where highly monodispersed drops are desirable while tip-streaming is used for the production of very small droplets (Christopher and Anna, 2007). These regimes depend on the physical properties of the fluids (i.e. interfacial tension and viscosity) (Tice et al., 2004), the linear velocity (Burns and Ramshaw, 1999) and the flowrates of the fluids (Zhao and Middelberg, 2011), the microchannel size, geometry (Kashid and Agar, 2007), material (Ahmed et al., 2006) and wettability (Asadi-Saghandi et al., 2021; Dessimoz et al., 2008).

Flow patterns are often shown in maps with coordinates such as phase flowrates, volume fraction or dimensionless numbers. The use of the latter allows the presentation of universal flow pattern maps, with $Ca = \frac{\mu u}{\gamma}$, $We = \frac{\varrho u^2 l}{\gamma}$ and $Re = \frac{\varrho u l}{\mu}$ most commonly used as axes (μ, ϱ, u, γ and l are viscosity, density, superficial velocity, interfacial tension and characteristic length, respectively). Cubaud and Mason (2008) identified five characteristic drop formation regimes for viscous fluids, which they named threading, jetting, dripping, tubing and displacement and presented them in a flow pattern map with the Ca numbers of the two phases as coordinates. In the same year, Dessimoz et al. (2008) studied drop formation in glass

microchannels with T- and Y-shaped inlets and developed a model to predict the boundaries of the flow regimes and the influence of fluid properties, based on mean Ca and Re numbers of each phase. For the dripping-to-jetting transition, Utada et al. (2007) found that it mainly depends on the Ca number based on the properties of the continuous phase and the We number based on the properties of the dispersed phase. Yagodnitsyna et al. (2016) replaced the We number with the product $WeOh$, where $Oh = \frac{\mu}{\sqrt{\varrho\gamma l}}$, to include the effect of viscous forces and proposed a generalized correlation for flow pattern transitions. Using $WeOh$ they were able to predict well the transitions in the flow patterns identified by Zhao et al. (2006). Darekar et al. (2017) also found that $WeOh$ is appropriate for presenting generalised liquid−liquid flow regime maps. Later on, Cao et al. (2018) studied experimentally four different liquid-liquid systems in a non-circular glass microchannel and presented clear transitions between the different drop formation patterns by using Re and We as coordinates. In a recent study, Asadi-Saghandi et al. (2021) performed experiments with six liquid-liquid systems in a microdevice with 4 microchannels with Y inlets. They were able to reduce the overlapping of the flow regimes from 10.1% to 3% by using $Ca^{0.31}$, $We^{0.07}$ and $We^{0.25}Oh^{0.31}$ as coordinates to the flow pattern maps.

Most available studies on the drop formation flow regimes in microchannels have been conducted with pure fluids (Asadi-Saghandi et al., 2021; Cao et al., 2018; Cubaud and Mason, 2008; Darekar et al., 2017; Dessimoz et al., 2008; Kashid and Agar, 2007; Lei et al., 2021; Mastiani et al., 2017; Salim et al., 2008; Shahriari et al., 2016; Tsaoulidis et al., 2013; Wu et al., 2017; Yagodnitsyna et al., 2016; Zhao et al., 2006), and only limited works have considered surfactants (Anna and Mayer, 2006; Carneiro et al., 2019; Fu et al., 2012; Kovalchuk et al., 2019, 2018b; Roumpea et al., 2019). Roumpea et al. (2019) and Kovalchuk et al. (2018b) identified 4 different regimes, including squeezing, dripping, threading and jetting flows, using silicone oil as the continuous phase and water-glycerol solutions with and without different

cationic surfactants as the dispersed phase. Results revealed a change of the flow regime boundaries upon the addition of surfactants, limiting the area of squeezing and dripping regimes on the flow pattern map to lower flowrates and extending the area of jetting and threading regimes to higher flowrates of both phases. More recently, Kovalchuk et al. (2019) observed a jetting-dripping-jetting transition with increasing continuous phase flowrate for the first time in a flow-focusing microfluidic device for surfactant concentrations well above the critical micelle concentration (CMC). They found that the critical value of the Ca for these transitions can be derived accurately only at moderate to high Ca, but not at low Ca. Anna and Mayer (2006) observed in a geometrically flow-focusing microchannel that the addition of $C_{12}E_8$ surfactant in the aqueous phase could affect the formation of fine threads only at concentrations above the CMC. A recent work discussed the importance of using appropriate dimensionless numbers when plotting flow pattern maps in systems with surfactants and specifically the dynamic interfacial tension; the use of $(Ca + We)$ of the dispersed phase and Ca of the continuous phase were recommended as map coordinates for concentrations above CMC (Du et al., 2020). Dinh et al. (2021) used the pendant drop method to measure the dynamic interfacial tension of slow adsorbing surfactants including Tween 20 and Span 80, which take about 2 mins to equilibrate. However, such techniques cannot be used for fast absorbing surfactants which equilibrate within milliseconds, since sample preparation times can be longer compared to surfactant diffusion and adsorption times (Kalli et al., 2022).

In this work we study the flow patterns of drops formed in another immiscible liquid in microfluidic channels for surfactants with different kinetics and concentrations below and above CMC. We show the effects of surfactant type and concentration on the boundaries of the dripping and jetting flow regimes and discuss thoroughly the drop formation times in terms of surfactant activities. We further present the results in a flow pattern map using as coordinates the Ca numbers of the two phases, which are based on equilibrium interfacial tension. This

approach would be reasonable for fast absorbing surfactants at high concentrations. However, as shown in previous work (Kalli et al., 2022), when using surfactants at low concentrations or with slow absorption kinetics, the concentration at the interface may not reach equilibrium during drop formation, especially at the early stages. For these cases, we recommend here to use the dynamic interfacial tension instead of the equilibrium one, which we obtain experimentally for the dripping and jetting regimes in the millisecond scale. Thus, we revise the map by using the dynamic interfacial tension to calculate the Ca numbers. We show for the first time that with the revised dimensionless numbers, universal transition boundaries can be drawn between the dripping and jetting regimes for all fluid systems studied, without and with surfactants at all concentrations.

2. MATERIALS, EXPERIMENTAL METHODS AND DATA PROCESSING

2.1 Materials and strength of surfactant

For the experiments we used a low viscosity silicone oil (Clearco) as the continuous phase and a mixture of 52% w/w glycerol solution (Sigma-Aldrich, ≥99.5%) as the dispersed phase in order to match the refractive index of the oil ($n_i = 1.39$ at 22°C). All solutions were prepared a few hours before each run, while experiments were repeated twice for validation. The physical properties of both phases are listed in **Table 1**.

Three surfactants were used, a cationic dodecyltrimethylammonium bromide (DTAB), an anionic sodium dodecylsulfate (SDS) and a non-ionic Triton X-100 (TX100), which were dissolved in the dispersed phase. The CMC values of DTAB, SDS and TX100 are 20mM, 11mM and 3.5mM, respectively. Surfactant concentrations below and above CMC were used, with C/CMC ranging from 0.1 – 8.6. The surfactant isotherms can be found in SI (Figure S1).

Table 1: Physical properties of the dispersed and continuous phases at 22°C

	Dispersed phase Aqueous glycerol solution (52% w/w)	**Continuous phase** Silicone oil
ρ (kg/m^3)	1132	920
μ (Pa s)	7	4.6
γ_{eq} (mN/m)	32.0	

Surfactants can be characterised by the surfactant strength parameter β, which is related to the interfacial tension, γ, at a certain surfactant concentration C, via the Langmuir-Frumkin equation of state (Frumkin, 1925):

$$\gamma = 1 + \beta\, ln\left(1 - \frac{\Gamma_{eq}}{\Gamma_{max}} C\right), \quad (\mathbf{1})$$

where Γ_{eq} is the equilibrium surfactant concentration on the interface, Γ_{max} is the surfactant concentration at a saturated interface, β (surfactant strength) is a dimensionless parameter equal to $\beta = \frac{\Gamma_{max} RT}{\gamma_0}$, γ_0 is the interfacial tension of the pure system without surfactant, *R* is the ideal gas constant and *T* is the absolute temperature. High β values indicate a large reduction in γ with surfactant concentration Γ_{eq} at the interface (Antonopoulou, 2020).

From interfacial tension measurements using a Du Noüy ring attached to a Force K100 Tensiometer (Krüss) in previous work (Kalli et al., 2022), the β value for each surfactant was calculated to be β_{DTAB} = 0.23, β_{SDS} = 0.18 and β_{TX100} = 0.10 (in agreement with Antonopoulou (2020)). Studies using dynamic measurements in the millisecond scale, report that surfactants with low CMC values reach equilibrium surface tension at a slower rate compared to surfactants with high CMC, because of the low surfactant molecule concentration in the bulk (Ferri and Stebe, 2000; Kovalchuk et al., 2018b). The above calculated surfactant strengths

follow the sequence of $\beta_{\mathrm{DTAB}} > \beta_{\mathrm{SDS}} > \beta_{\mathrm{TX100}}$, in agreement with the CMC values of the surfactants studied here which reduce as follows $\mathrm{CMC_{DTAB}} > \mathrm{CMC_{SDS}} > \mathrm{CMC_{TX100}}$.

2.2 Experiments on drop formation

The regimes of drop formation were studied in a glass flow-focusing microchannel with a main channel equal to 390 μm × 190 μm (width × depth) and side channels equal to 195 μm × 190 μm (width × depth), as shown in **Figure 1** (Dolomite Microfluidics, UK). The two liquids were driven into the test section via two syringe pumps (KDS Scientific); in the experiments the silicone oil was pumped first and formed the continuous phase, while the glycerol solution was added afterwards and formed the dispersed phase. For the imaging of the flow patterns a 12-bit high-speed camera (Photron, 1280 × 800 pixels resolution) was used at a frequency of 10000fps, equipped with a Nivatar 12x zoom lens, while illumination was provided by an LED background light. The continuous phase flowrate was kept constant in each run (0.003 mL/min $\leq Q_c \leq$ 0.2 mL/min), while the dispersed phase flowrate (0.01 mL/min $\leq Q_d \leq$ 0.4 mL/min) was increased at increments of 0.02 mL/min. An in-house MATLAB (R2017b) code was used to detect the liquid-liquid interface and to obtain the drop formation times in the dripping and jetting regimes, which are defined as the number of frames from the pinch-off of a drop until the detachment of the following drop, divided by the frame rate of the camera. The experimental error (0.1ms) is shown using error bars on the following graphs; it was found that the standard deviation increased with surfactant addition and Q_d/Q_c ratio, ranging from 0.8% – 5.2% in the pure case to 0.6% – 18.2% in the surfactant cases. The reason behind this increase will be further discussed in **Section 3.2**.

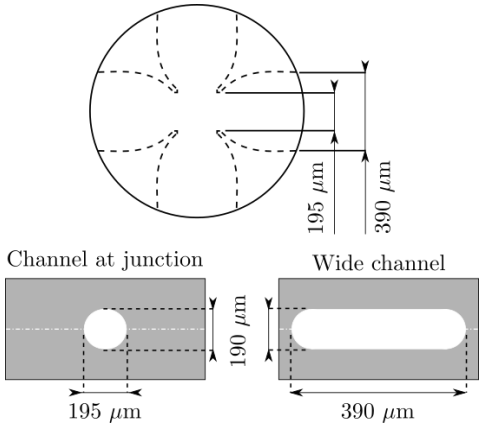

Figure 1. Schematic of the flow-focusing microchannel with relevant dimensions shown

3. RESULTS AND DISCUSSION

3.1 Drop formation regimes in the presence of surfactants

Figure 2A illustrates the drop formation regimes in the flow focusing microchannel, namely squeezing, dripping, jetting and threading. In addition, when surfactants are present, a transition between the tip streaming and jetting regimes is also observed. As previously reported by several authors (Garstecki et al., 2005; Kiratzis et al., 2021; Roumpea et al., 2019), the squeezing and dripping regimes are typically divided into three stages called expansion, necking and pinch-off (**Figure 2B**) respectively. In each image, the dispersed phase is the aqueous solution, while the continuous phase is the organic silicone oil. The effect of TX100 surfactant on the jet pinch-off point is presented in **Figure 2C**. The flow pattern map for the system without surfactant is shown in **Figure 3**. In the same figure the flow pattern transition boundaries are shown when SDS is added at C/CMC = 1.0.

3.1.1 Pure system without surfactant

At low flowrates of both phases, 0.006 mL/min ≤ Q_c ≤ 0.02 mL/min and 0.01 mL/min ≤ Q_d ≤ 0.04 mL/min, the squeezing regime exists (**Figure 2A**(I); **Figure 3)**. At these low flowrates, the dispersed phase has time to grow and form a plug with a characteristic length larger than the inside channel width (l > 390 μm). As reported by Garstecki et al. (2005), a

geometry with an inlet width at least half of the main channel width, as is in this case, will result in the squeezing regime. In this regime, the drop detachment is caused by the pressure build-up behind the plug as it forms and blocks the cross-junction inlet; the continuous phase "squeezes" the plug neck until pinch-off (Anna, 2016; Garstecki et al., 2006).

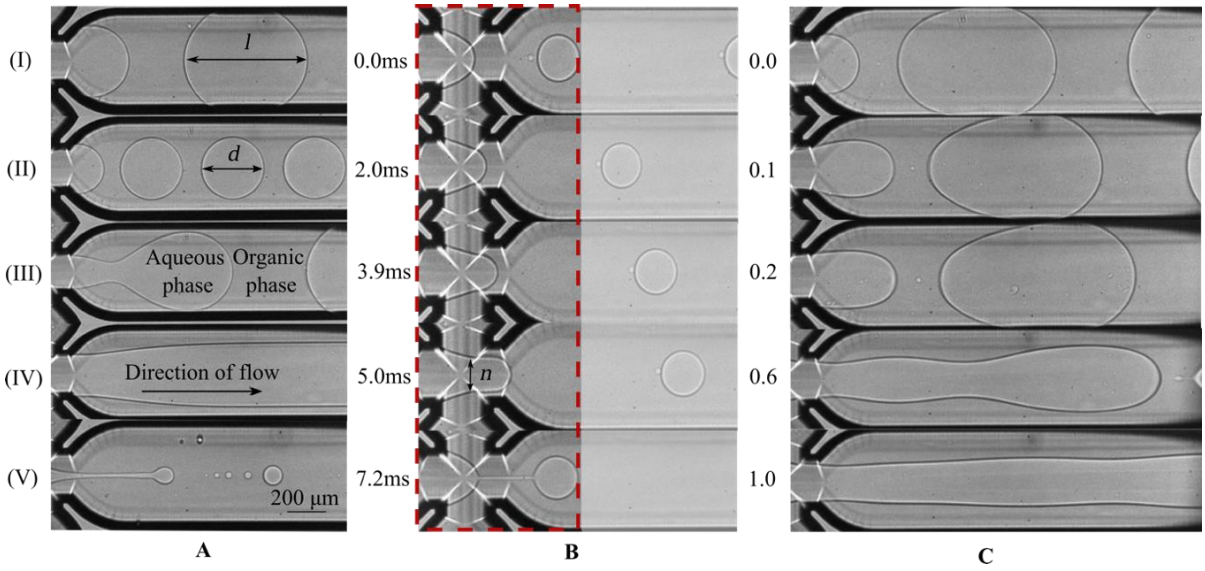

Figure 2. **(A)** Different drop formation flow patterns and drop formation stages in the flow-focusing microchannel: (I) squeezing (II) dripping (III) jetting (IV) threading (V) tip streaming/jetting. **(B)** Roman numbers indicate (I) - (II) Expansion stage from 0.0 ms – 2.0 ms, (III) - (IV) Necking stage from 3.9 ms – 5.0 ms, (V) Pinch-off point at 7.2ms; l is the plug length, d is the axial droplet diameter immediately after break-up and n is the neck width. Dashed rectangle shows the cross-junction inlet. **(C)** Effect of TX100 addition on flow patterns for Q_c = 0.08 mL/min and Q_d = 0.08 mL/min with C/CMC of (I) 0.0 (II) 0.1 (III) 0.2 (IV) 0.6 (V) 1.0

The dripping regime (**Figure 2A**(II)) is observed for 0.02 mL/min $\leq Q_c \leq$ 0.4 mL/min and 0.01 mL/min $\leq Q_d \leq$ 0.1 mL/min (**Figure 3**). In this regime, the dispersed phase acquires a circular shape and the drops have a diameter smaller than the channel width (d < 390 µm). The drop detachment is controlled by the balance between interfacial tension and viscous shear forces (Wang et al., 2009) while the formed drops do not obstruct the flow entirely. If the length

of drops is between 190 μm and 390 μm, then they are not spherical (pancake shape, Kovalchuk et al., 2018b).

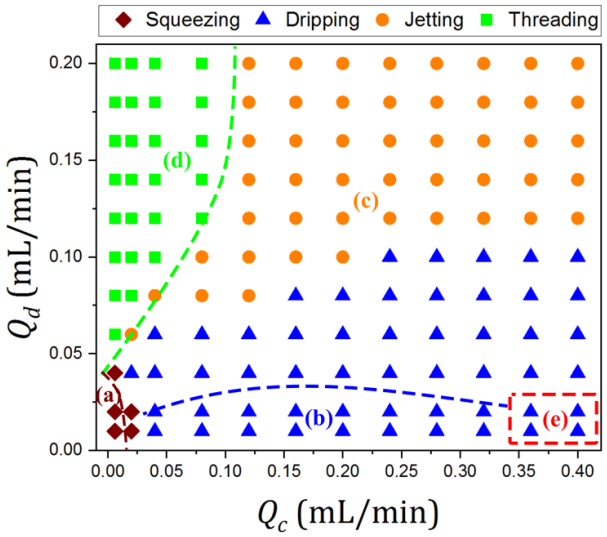

Figure 3. Drop formation flow pattern map of the pure system without surfactants. The dashed lines show the flow regime boundaries when the SDS surfactant is added at C/CMC = 1 (a) squeezing regime (b) dripping regime (c) jetting regime (d) threading regime and (e) tip streaming/jetting transition regime

When the flowrates of both phases are increased, there is a transition to the jetting regime (**Figure 3** and **Figure 2A**(III)), within 0.02 mL/min ≤ Q_c ≤ 0.4 mL/min and 0.06 mL/min ≤ Q_d ≤ 0.2 mL/min. The additional drag force from the increased continuous phase flowrate competes with the interfacial tension force and pushes the dispersed phase downstream, to form a jet. As observed by Kovalchuk et al. (2018b), the jet length increases with decreasing interfacial tension. The critical jet length before pinch-off is proportional to the visco-capillary time scale, $t_{cap} = R_c\mu/\gamma$, where R_c is the channel radius; this time scale is inversely proportional to the interfacial tension. The increase of the jet length with the addition of TX100 surfactant is evident in **Figure 2C**. A shift of the pinch-off point further downstream from the inlet at high dispersed phase flowrates is also observed, in agreement with Utada et al. (2007) and Roumpea et al. (2019).

On the other hand, an increase in Q_d at a low Q_c results in the threading regime (**Figure 3** and **Figure 2A**(IV)), where the dispersed phase forms a stable thread, surrounded by a thin film of the continuous phase. As expected, the width of the thread increases with Q_d.

In applications where monodispersed droplets are required, drop generators mainly operate within the squeezing and dripping regimes (Tostado et al., 2012; Wang et al., 2016; Xu et al., 2008). The formation process associated with these regimes is divided into 3 stages called expansion, necking and pinch-off. As proposed by Garstecki et al. (2006), these stages will depend on the competition between the interfacial tension force and the combination of shear stress and pressure gradient forces in the continuous oil phase. The expansion stage starts immediately after the previous drop has detached, where the interface slightly pulls backwards into the inlet, before it starts expanding forward into the main channel again. Initially, the drop grows in all directions and is mainly dominated by the interfacial tension force, forming a parabolic interface profile as shown by **Figure 2B**(I). Later on, the drop expands axially towards the main channel, until the edge of the cross junction (**Figure 2B**(II)). At this point, the profile of the interface front is still parabolic. The growing dispersed phase restricts the side inlet flow of the continuous oil phase causing a pressure build-up, which eventually overcomes the interfacial tension forces and causes a reversal of the interface curvature at the neck in the junction, indicating the beginning of the neck thinning stage (**Figure 2B**(III-IV)). During this stage, the neck width (n; shown in **Figure 2B**(IV)) starts to decrease until pinch-off and drop detachment (**Figure 2B**(V)). Similar observations were also made in flow-focusing devices by Roumpea et al. (2019) and in T-junction inlets by Glawdel and Ren (2012) and Chinaud et al. (2016).

3.1.2 Systems with surfactants

The drop formation patterns were also studied when surfactants were added in the aqueous phase. Higher flowrates than in previous works in similar systems (Kovalchuk et al., 2018b; Roumpea et al., 2019) were used and a transition between tip streaming and jetting was observed, as shown in **Figure 2A**(V). This instability is common in flow-focusing droplet generators with surface active agents and is attributed to the accumulation of the surfactants on the emerging drop tip, which causes concentration gradients along the interface (Anna and Mayer, 2006; Leal and Stone, 1990). In this regime, the neck acquires a conical shape while a thin dispersed phase thread forms which breaks into a drop followed by much smaller satellite drops, as seen in **Figure 2A**(V). The drops formed in this regime are significantly smaller (d < 80 μm) than in the other ones. Satellite drops have also been observed with increasing concentration of surfactant (Kovalchuk et al., 2018a) and will be further explored later.

The flow pattern transition boundaries using SDS at C/CMC = 1 are indicated by dashed lines in **Figure 3**. As can be seen, the boundaries shift with the addition of the surfactant, especially the transition from the dripping to the jetting regime. The squeezing regime (a) is restricted to low flowrates of both phases (Q_c = 0.006 mL/min and 0.01 mL/min ≤ Q_d ≤ 0.02 mL/min), while the dripping regime (b) mainly appears at low dispersed phase flowrates (0.04 mL/min ≤ Q_c ≤ 0.32 mL/min and 0.01 mL/min ≤ Q_d ≤ 0.02 mL/min). The jetting regime (c) expands to low dispersed phase flowrates (0.02 mL/min ≤ Q_c ≤ 0.4 mL/min and 0.04 mL/min ≤ Q_d ≤ 0.2 mL/min) while the threading regime (d) extends slightly to higher continuous phase flowrates (0.006 mL/min ≤ Q_c ≤ 0.12 mL/min and 0.04 mL/min ≤ Q_d ≤ 0.2 mL/min) compared to the pure case. The tip streaming/jetting transition regime (e) is predominant at high continuous phase and low dispersed phase flowrates (0.36 mL/min ≤ Q_c ≤ 0.4 mL/min and 0.01 mL/min ≤ Q_d ≤ 0.02 mL/min).

The effect of the surfactant concentration on the dripping regime boundaries can be seen in **Figure 4**(a), (b) and (c) for the DTAB, SDS and TX100 surfactants respectively. A clear reduction of the dripping regime area in the map with increasing surfactant concentration is observed for all three surfactants. As seen in **Figure 4**(c), the flow pattern map changes significantly at high TX100 concentrations with a small dripping regime area only, observed at C/CMC = 8.6. At surfactant concentrations C/CMC = 1, TX100 gives the largest dripping regime area compared to DTAB and SDS**.** This is attributed to the low value of β_{TX100} = 0.10 compared to β_{SDS} = 0.18 and β_{DTAB} = 0.2.

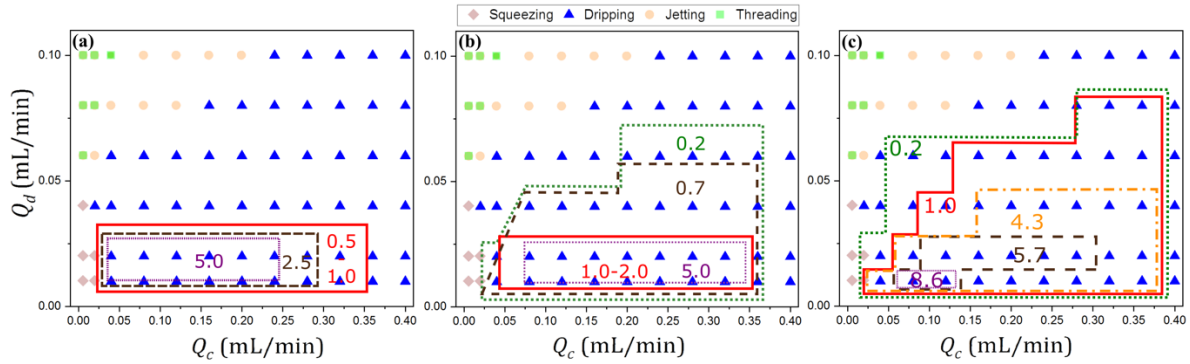

Figure 4. Effect of surfactant concentration on the drop formation flow pattern map. The boundaries of the dripping regime are shown for (a) DTAB, solid line at C/CMC = 0.5 and 1.0, dashed line at C/CMC = 2.0 and shadow line at C/CMC = 5.0 (b) SDS, dotted line at C/CMC = 0.2, dashed line at C/CMC = 0.7, solid line at C/CMC = 1.0 and 2.0 and shadow line at C/CMC = 5.0 (c) TX100 dotted line at C/CMC = 0.2, solid line at C/CMC = 1.0, dot-dash line at C/CMC = 4.3, dashed line at C/CMC = 5.7 and shadow line at C/CMC = 8.6

Both jetting and jetting/tip-streaming regimes can have either alternating drops with large and small sizes (**Figure 5**(b)) or satellite drops after the main one (**Figure 5**(c)). Formation of satellite drops is observed at all surfactant concentrations (**Figure 5**). The presence of surfactant prevents coalescence of the small drops with the main one, as opposed to the pure case where the satellite drops disappear as they travel downstream into the main channel. The

size of satellite drops increases at high concentrations of all surfactants as also observed in previous works (Craster et al., 2009; Kovalchuk et al., 2016), where it is believed that Marangoni stresses can cause formation of large satellite droplets at high surfactant concentrations. Additionally, multiple satellite drops are observed at very low Q_d as shown in **Figure 5**(c).

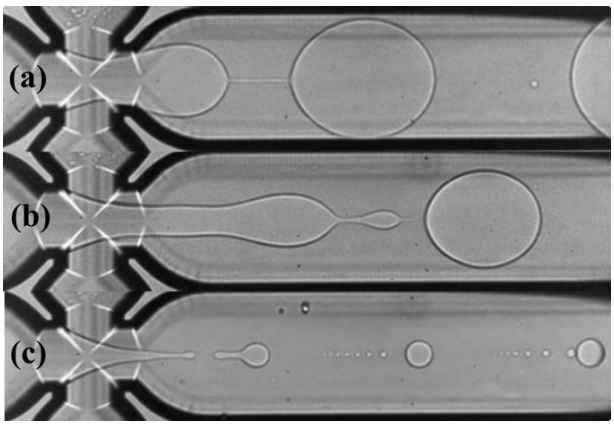

Figure 5: Formation of satellite drops at different flowrates and surfactant concentrations with (a) SDS at C/CMC = 0.2, Q_c = 0.16 mL/min and Q_d = 0.08mL/min (b) DTAB at C/CMC = 2.5, Q_c = 0.16 mL/min and Q_d = 0.04mL/min (c) TX100 at C/CMC = 8.6, Q_c = 0.16 mL/min and Q_d = 0.003 mL/min

The evolution of the jetting regime area in the map upon addition of the TX100 surfactant is shown in **Figure 6**. The area is reduced to low Q_c and Q_d flowrates as C/CMC increases from 0.2 to 5.7. A similar trend is observed with the rest of the surfactants. This observation validates the importance of surfactants in applications such as inkjet printing, where the reduced interfacial tension can result in lower power requirements for the actuation signal (Antonopoulou, 2020).

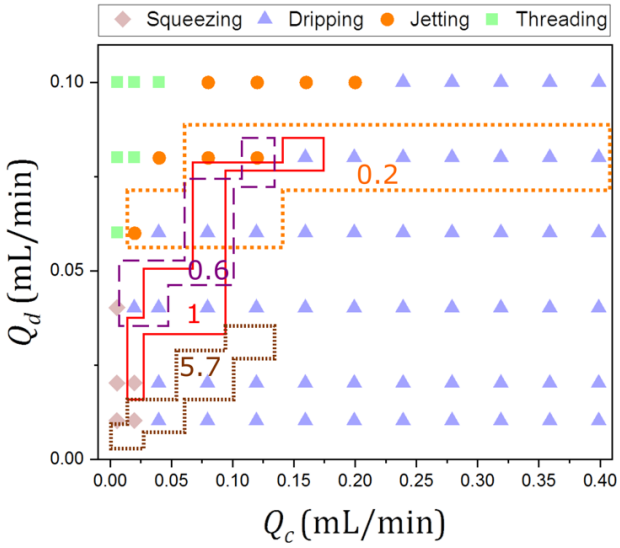

Figure 6: Changes of the jetting regime boundaries with TX100 concentration. Dotted line at C/CMC = 0.2, dashed line at C/CMC = 0.7, solid line at C/CMC = 1.0 and shadow line at C/CMC = 5.7

3.2 Drop pinch-off point in the jetting regime

By increasing the surfactant concentration and/or the dispersed to continuous phase flowrate ratio (Q_d/Q_c), a shift of the drop pinch-off point in the jetting regime is observed further downstream from the inlet (see **Figure 2C**, for increasing ratio c/CMC TX100). Kovalchuk et al. (2018b) found a shift of the pinch-off point with increasing Q_d/Q_c and noted an increase of the jet length when surfactants are added, which is proportional to $t_{cap} = R_c\mu/\gamma$. A similar observation was made by Utada et al. (2007), who studied the transition from dripping to jetting regimes in co-flowing liquids. They proposed that the higher inertia force at increased dispersed phase flowrates acting cooperatively with the drag force from the continuous phase, shifts the pinch-off point of the drop further downstream into the main channel.

The uneven surfactant distribution at the interface at high surfactant concentrations will cause large interfacial tension gradients and alter the position of the pinch-off point, resulting in a distribution of drop sizes (Kovalchuk et al., 2019) (**Figure 7**(b)-(c) where SDS and TX100 were used at $C/CMC = 1.4$, respectively) as opposed to the pure case (**Figure 7**(a)), where the

pinch-off point always happens at the same position in the channel and similar drops form. This justifies the higher standard deviation values in the surfactant-laden cases as reported in **Section 2.2**.

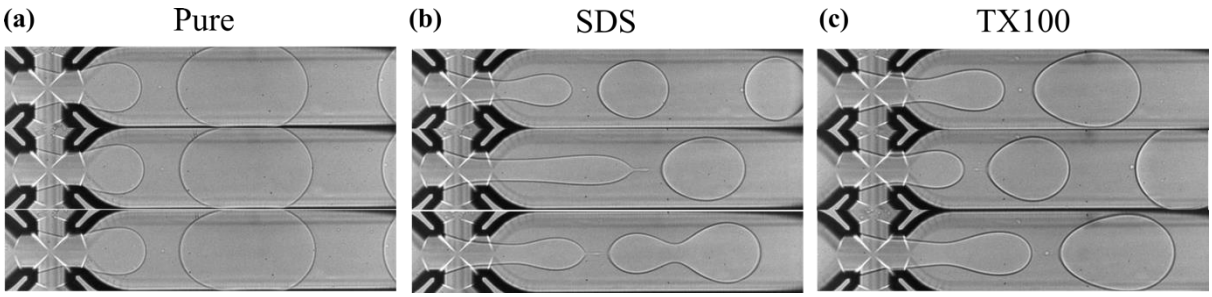

Figure 7: (a) Pure (b) SDS at C/CMC = 1.4 and (c) TX100 at C/CMC = 1.4

3.3 Drop formation time

The surfactant concentration at the interface may not reach equilibrium values during the drop formation, because the formation times are faster than the time required for the surfactant to transfer and absorb to the interface (Du et al., 2020). Dynamic interfacial tension values should then be used instead of the equilibrium ones in the dimensionless numbers that are used to describe the flow patterns. Microfluidic approaches have used to derive dynamic interfacial tension values at relevant timescales of drop formation (Kalli et al., 2022; Moiré et al., 2017; Wang et al., 2016). In this section, the drop formation time in the dripping (t_{drip}) and jetting (t_{jet}) regimes will be presented at different Q_d/Q_c and C/CMC ratios. From these, the corresponding dynamic interfacial tension values will be derived, which will then be used to calculate modified dimensionless numbers and plot a universal flow pattern map.

3.3.1 Drop formation time in the dripping regime

As shown in **Figure 8** for DTAB, the drop formation time in the dripping regime, t_{drip}, increases with increasing Q_d/Q_c ratio as the shear force from the continuous phase decreases, while it decreases with increasing C/CMC ratio because interfacial tension forces decrease. The slopes of the fitted lines (m) decrease from 242.5 to 76.5 as the C/CMC ratio increases

from 0.0 to 1.0; above CMC the lines collapse to a single curve and the slope reaches a plateau with m = 76.2, which denotes that the equilibrium interfacial tension has been reached (Kalli et al., 2022). In order to better understand surfactant dynamics during each stage of the drop formation, the expansion (t_{exp}) and necking times (t_{neck}) were also measured. In the pure system without surfactant, the expansion time is the main contributor to the drop formation time, at all continuous phase flowrates. However, when surfactants were added, the contribution of the necking time to the overall drop formation time became significant as can be seen in **Figure 9**, while at very low continuous phase flowrates ($Q_c \leq 0.04$ mL/min) it even exceeded the expansion time. At such low continuous phase flowrates, the regime changes from dripping to squeezing. This has also been reported by Roumpea et al. (2019), who found that in the squeezing regime the necking stage is longer than the expansion stage in the presence of surfactants. Interestingly, for DTAB and SDS surfactants, this happens at concentrations above the CMC value (C/CMC = 2.5 and 2.0 respectively), while for the TX100 surfactant, this is observed at low concentrations, at C/CMC = 0.6. This might be attributed to TX100 showing a sharper decrease in interfacial tension at low surfactant concentrations (Ferri and Stebe, 2000; Kovalchuk et al., 2016) as opposed to DTAB and SDS (See **Figure S1** in SI). Similar findings were observed from numerical simulations (Antonopoulou, 2020; Constante-Amores et al., 2021; Cui and Gupta, 2012) where the presence of surfactants makes interfaces more rigid, slows down the neck growth and extends the necking stage.

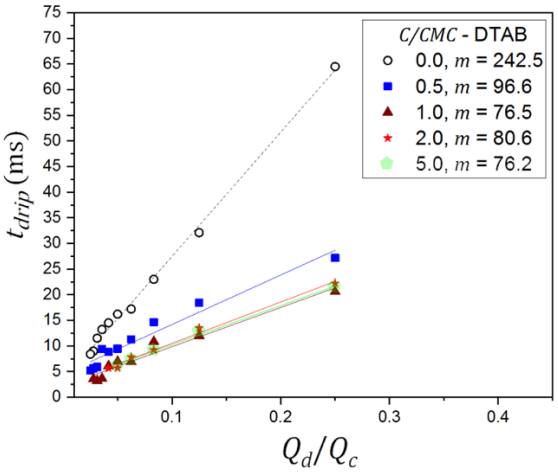

Figure 8. (a) Effect of Q_d/Q_c and DTAB surfactant concentration on the drop formation time in the dripping regime t_{drip} at Q_d = 0.01 mL/min

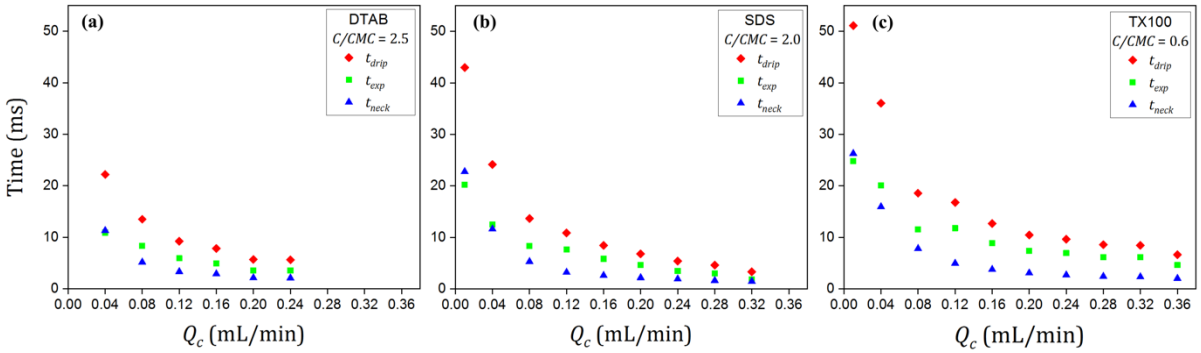

Figure 9. Expansion and necking times of drop formation in the dripping regime against continuous phase flowrate at Q_d = 0.01 mL/min for (a) DTAB at C/CMC = 2.5, (b) SDS at C/CMC = 2.0 and (c) TX100 at C/CMC = 0.6

3.3.2 Drop formation time in the jetting regime

The effect of the dispersed to continuous phase flowrate ratio (Q_d/Q_c) on the drop formation time in the jetting regime (t_{jet}), at different concentrations of the three surfactants is shown in **Figure 10**. As it can be seen, t_{jet} increases with increasing Q_d/Q_c ratio because of the reduced effect of the shear force from the continuous phase. In contrast to the dripping regime, t_{jet} increases with increasing C/CMC ratio. As it can be seen from **Figure 10**, the slopes of the

fitted lines increase with C/CMC ratio from m = 15.1 for the pure case to m = 31.8 for DTAB at C/CMC = 2.5, m = 45.1 for SDS at C/CMC = 1.4 and m = 43.4 for TX100 at C/CMC = 2; beyond these concentrations, the slopes reach a plateau and do not change further. The t_{jet} data points are less at high C/CMC ratios due to the change in the flow pattern as shown in **Figure 6**. Similarly to the dripping regime, m for TX100 does not reach a plateau as in the DTAB and SDS cases due to the differences in surfactant kinetics as explained in previous work (Kalli et al., 2022). Contrary to t_{drip}, the t_{jet} is inversely proportional to interfacial tension and increases with surfactant concentrations. This is attributed to changes in the relevant forces acting in the two regimes (Cubaud and Mason, 2008). As mentioned in **Section 3.1.1**, the dripping regime is dominated by interfacial tension and viscous shear forces, so a lower interfacial tension at increased surfactant concentrations (higher C/CMC ratio) will result in faster drop detachment, as shown in **Figure 8**. In contrast, in the jetting regime a cylindrical jet is formed that then breaks into smaller drops. As a result, Marangoni effects caused by interfacial concentration gradients at the neck can delay interface break-up (Antonopoulou, 2020).

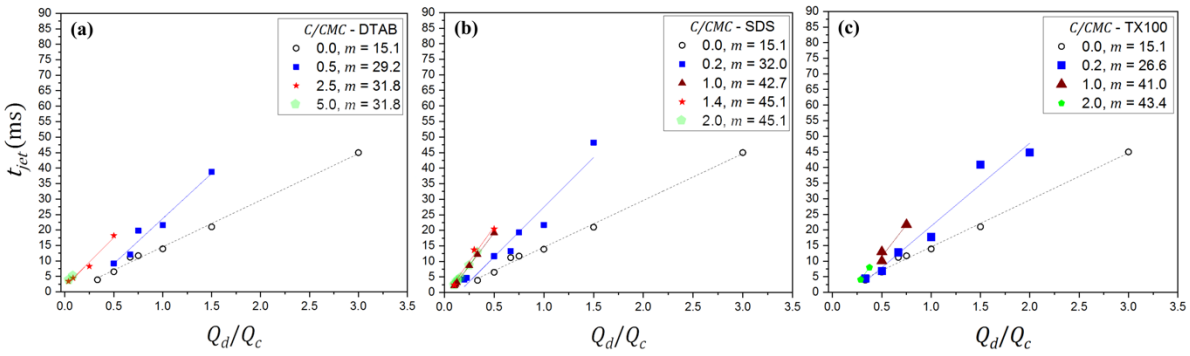

Figure 10: Effect of Q_d/Q_c and surfactant addition on jet formation time for (a) DTAB (b) SDS (c) TX100. Q_d varies in the range of 0.01 – 0.12 mL/min depending on each surfactant

The effect of β on t_{jet} is shown in **Figure 11** for dispersed phase flowrates in the range of 0.06 mL/min $\leq Q_d \leq$ 0.12 mL/min. The t_{jet} for TX100 with β_{TX100} = 0.10 is closer to that of the pure case compared to SDS with β_{SDS} = 0.18. Antonopoulou (2020) compared numerical

simulations of a weak ($\beta = 0.1$, low CMC) and a strong surfactant ($\beta = 1$, high CMC) during jet-break up for inkjet printing applications. It was found that in the strong surfactant case, the large surfactant concentration gradients close to the neck resulted in high interfacial tension gradients as opposed to the weaker surfactant case. This caused a strong Marangoni force away from the forming drop and towards the dispersed phase neck, which could prevent jet break-up and increase t_{jet} (Antonopoulou et al., 2021). This possibly explains why SDS has longer t_{jet} than TX100 at C/CMC = 0.2 (**Figure 11**). The effect of the activity of the surfactants is reflected on the slope, m, of the t_{jet} versus Q_d/Q_c curves with m = 32.0 for the strong SDS surfactant being larger than m = 26.6 for the less active TX100.

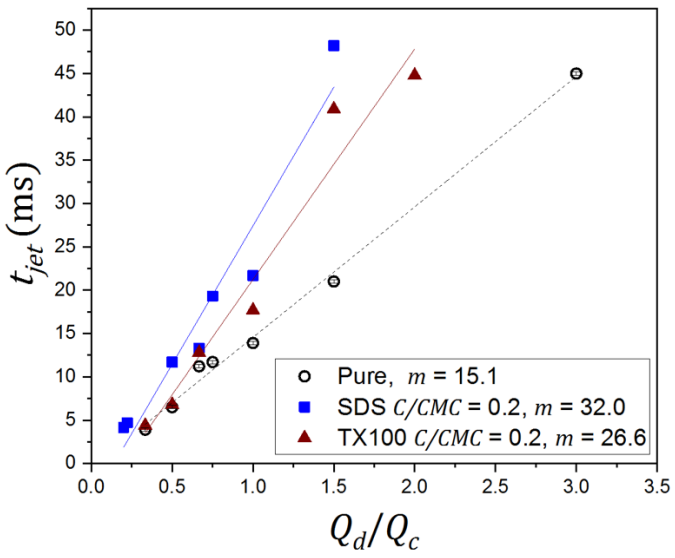

Figure 11: Effect of a strong (SDS) and a weak (TX100) surfactant on the drop formation times in the jetting regime for $0.06 \leq Q_d \leq 0.12$ mL/min.

3.4 Universal flow pattern map

Using the above drop formation times in the dripping and jetting regimes, the corresponding dynamic interfacial tension values were obtained (Kalli et al., 2022). The flow pattern maps for the dripping and jetting regimes were firstly plotted using the capillary numbers ($Ca = \mu u_c/\gamma$, where $u_c = Q_c/A_{inlet}$, and A_{inlet} is the area corresponding to the cross-sectional area

of the inlet junction) of the dispersed (Ca_d) and continuous (Ca_c) phases based on the equilibrium interfacial tension values. They are presented in **Figure 12** (a) for the pure system (closed symbols) and the surfactant systems at all concentrations (open symbols). As it can be seen there is an overlap of the dripping and jetting regimes and no clear transition boundary. On the contrary, when the dynamic interfacial tension values are used, the regimes for all cases, including pure and surfactant solutions, collapse into separate regions and a universal transition boundary between the dripping and jetting regimes can be drawn (**Figure 12**(b)).

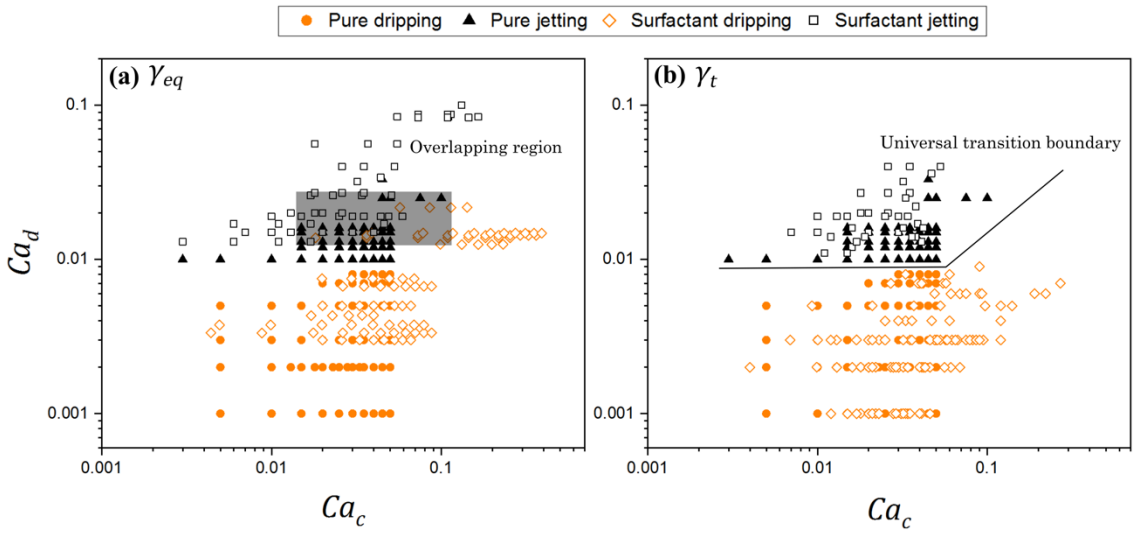

Figure 12: Dripping and jetting drop formation pattern maps with the capillaries of the continuous (Ca_c) and the dispersed (Ca_d) phases as coordinates. a) equilibrium interfacial tension (γ_{eq}) is used; b) dynamic interfacial tension (γ_t) is used.

4. CONCLUSIONS

Drop formation was studied experimentally in a flow focusing microfluidic channel using silicone oil as the continuous phase and surfactant-laden aqueous solutions with 52% w/w glycerol as the dispersed phase. The effect of surfactant concentration below and above CMC

on the flow pattern maps of drop formation was studied for three surfactants, DTAB, SDS and Triton X-100 (TX100).

Five drop formation flow patterns were observed namely squeezing, dripping, jetting, threading and tip streaming/jetting, with the latter formed only when surfactants were used. When surfactants were used, the areas on the flow pattern map, with the flowrates of the two phases as coordinates, reduced for the squeezing and dripping regimes, while the jetting and threading regimes were extended. For the squeezing and dripping patterns, the different stages during droplet formation were identified as expansion, necking and pinch-off. The formation times of drops in the dripping and jetting regimes decreased when the flowrate of the continuous oil phase was increased due to increased shear stresses. However, the effect of surfactants on the drop formation time between the two regimes was the opposite. An increasing surfactant concentration decreased the drop formation time in the dripping regime (t_{drop}) but increased it in the jetting regime (t_{jet}). The effect of the C/CMC ratio was analysed quantitatively with the slopes of the fitted lines (m) which decreased for t_{drop} and increased for t_{jet} until they reached a plateau, where the curves collapse.

When plotted in maps using as coordinates the capillary numbers (Ca) of the two phases based on the equilibrium interfacial tensions, an overlap of the dripping and jetting regimes was found. However, when dynamic interfacial tensions were used in the calculation of Ca, the transition boundaries between the dripping and the jetting regimes collapsed in the revised flow pattern maps for all systems considered, including the three surfactants at different concentrations and the pure system with no surfactants.

In future work we will investigate the velocity fields and circulation patterns during drop formation using novel particle image velocimetry techniques (Roumpea et al., 2019) and compare with numerical simulations.

ACKNOWLEDGMENTS

The authors would like to acknowledge support from the UK Engineering and Physical Sciences Research Council (EPSRC) Programme Grant PREMIERE (EP/T000414/1). M Kalli would also like to acknowledge the EPSRC Doctoral Training Programme (EP/R513143/1) for her studentship.

ABBREVIATIONS

CMC, critical micelle concentration.

References

Ahmed, B., Barrow, D., Wirth, T., 2006. Enhancement of reaction rates by segmented fluid flow in capillary scale reactors. Adv. Synth. Catal. 348, 1043–1048. https://doi.org/10.1002/adsc.200505480

Anna, S.L., 2016. Droplets and Bubbles in Microfluidic Devices. Annu. Rev. Fluid Mech. 48, 285–309. https://doi.org/10.1146/annurev-fluid-122414-034425

Anna, S.L., Mayer, H.C., 2006. Microscale tipstreaming in a microfluidic flow focusing device. Phys. Fluids 18. https://doi.org/10.1063/1.2397023

Antonopoulou, E., 2020. The Role of Surfactants in Jet Break-Up for Inkjet Printing. University of Leeds.

Antonopoulou, E., Harlen, O.G., Rump, M., Segers, T., Walkley, M.A., 2021. Effect of surfactants on jet break-up in drop-on-demand inkjet printing. Phys. Fluids 33. https://doi.org/10.1063/5.0056803

Asadi-Saghandi, H., Karimi-Sabet, J., Ghorbanian, S., Ali Moosavian, S.M., 2021. Dimensionless analysis on liquid-liquid two-phase flow patterns in a numbered-up microfluidic device. Chem. Eng. J. 132428. https://doi.org/10.1016/j.cej.2021.132428

Burns, J.R., Ramshaw, C., 1999. Development of a microreactor for chemical production. Chem. Eng. Res. Des. 77, 206–211. https://doi.org/10.1205/026387699526106

Cao, Z., Wu, Z., Sundén, B., 2018. Dimensionless analysis on liquid-liquid flow patterns and scaling law on slug hydrodynamics in cross-junction microchannels. Chem. Eng. J. 344, 604–615. https://doi.org/10.1016/j.cej.2018.03.119

Carneiro, J., Campos, J.B.L.M., Miranda, J.M., 2019. PDMS microparticles produced in PDMS microchannels under the jetting regime for optimal optical suspensions. Colloids Surfaces A Physicochem. Eng. Asp. 580. https://doi.org/10.1016/j.colsurfa.2019.123737

Chinaud, M., Voulgaropoulos, V., Angeli, P., 2016. Surfactant effects on the coalescence of a drop in a Hele-Shaw cell. Phys. Rev. E 94, 1–11. https://doi.org/10.1103/PhysRevE.94.033101

Christopher, G.F., Anna, S.L., 2007. Microfluidic methods for generating continuous droplet streams. J. Phys. D. Appl. Phys. 40. https://doi.org/10.1088/0022-3727/40/19/R01

Constante-Amores, C.R., Batchvarov, A., Kahouadji, L., Shin, S., Chergui, J., Juric, D., Matar, O.K., 2021. Role of surfactant-induced Marangoni stresses in drop-interface coalescence. J. Fluid Mech. 925, 1–21. https://doi.org/10.1017/jfm.2021.682

Craster, R. V., Matar, O.K., Papageorgiou, D.T., 2009. Breakup of surfactant-laden jets above the critical micelle concentration. J. Fluid Mech. 629, 195–219. https://doi.org/10.1017/S0022112009006533

Cubaud, T., Mason, T.G., 2008. Capillary threads and viscous droplets in square microchannels. Phys. Fluids 20. https://doi.org/10.1063/1.2911716

Cui, Y., Gupta, N.R., 2012. Surfactant effects on drop formation in co-flowing fluid streams. Colloids Surfaces A Physicochem. Eng. Asp. 393, 111–121. https://doi.org/10.1016/j.colsurfa.2011.11.008

Darekar, M., Singh, K.K., Mukhopadhyay, S., Shenoy, K.T., 2017. Liquid-Liquid Two-Phase

Flow Patterns in Y-Junction Microchannels. Ind. Eng. Chem. Res. 56, 12215–12226. https://doi.org/10.1021/acs.iecr.7b03164

Dessimoz, A.L., Cavin, L., Renken, A., Kiwi-Minsker, L., 2008. Liquid-liquid two-phase flow patterns and mass transfer characteristics in rectangular glass microreactors. Chem. Eng. Sci. 63, 4035–4044. https://doi.org/10.1016/j.ces.2008.05.005

Dinh, H.H.Q., Santanach-Carreras, E., Lalanne-Aulet, M., Schmitt, V., Panizza, P., Lequeux, F., 2021. Effect of a Surfactant Mixture on Coalescence Occurring in Concentrated Emulsions: The Hole Nucleation Theory Revisited. Langmuir 37, 8726–8737. https://doi.org/10.1021/acs.langmuir.1c00975

Du, J., Ibaseta, N., Guichardon, P., 2020. Generation of an O/W emulsion in a flow-focusing microchip: Importance of wetting conditions and of dynamic interfacial tension. Chem. Eng. Res. Des. 159, 615–627. https://doi.org/10.1016/j.cherd.2020.04.012

Ferri, J.K., Stebe, K.J., 2000. Which surfactants reduce surface tension faster? A scaling argument for diffusion-controlled adsorption. Adv. Colloid Interface Sci. 85, 61–97. https://doi.org/10.1016/S0001-8686(99)00027-5

Frumkin, A.N., 1925. Electrocapillary curve of higher aliphatic acids and the state equation of the surface layer. Z. Phys. Chem. 116, 466–470.

Fu, T., Wu, Y., Ma, Y., Li, H.Z., 2012. Droplet formation and breakup dynamics in microfluidic flow-focusing devices: From dripping to jetting. Chem. Eng. Sci. 84, 207–217. https://doi.org/10.1016/j.ces.2012.08.039

Garstecki, P., Fuerstman, M.J., Stone, H.A., Whitesides, G.M., 2006. Formation of droplets and bubbles in a microfluidic T-junction - Scaling and mechanism of break-up. Lab Chip 6, 437–446. https://doi.org/10.1039/b510841a

Garstecki, P., Stone, H.A., Whitesides, G.M., 2005. Mechanism for flow-rate controlled breakup in confined geometries: A route to monodisperse emulsions. Phys. Rev. Lett.

94, 1–4. https://doi.org/10.1103/PhysRevLett.94.164501

Glawdel, T., Ren, C.L., 2012. Droplet formation in microfluidic T-junction generators operating in the transitional regime. III. Dynamic surfactant effects. Phys. Rev. E - Stat. Nonlinear, Soft Matter Phys. 86, 1–9. https://doi.org/10.1103/PhysRevE.86.026308

Kalli, M., Chagot, L., Angeli, P., 2022. Comparison of surfactant mass transfer with drop formation times from dynamic interfacial tension measurements in microchannels. J. Colloid Interface Sci. 605, 204–213. https://doi.org/10.1016/j.jcis.2021.06.178

Kashid, M.N., Agar, D.W., 2007. Hydrodynamics of liquid-liquid slug flow capillary microreactor: Flow regimes, slug size and pressure drop. Chem. Eng. J. 131, 1–13. https://doi.org/10.1016/j.cej.2006.11.020

Kiratzis, I., Kovalchuk, N.M., Simmons, M.J.H., Vigolo, D., 2021. Effect of surfactant addition and viscosity of the continuous phase on flow fields and kinetics of drop formation in a flow-focusing microfluidic device. Chem. Eng. Sci. 248, 117183. https://doi.org/10.1016/j.ces.2021.117183

Kovalchuk, N.M., Jenkinson, H., Miller, R., Simmons, M.J.H., 2018a. Effect of soluble surfactants on pinch-off of moderately viscous drops and satellite size. J. Colloid Interface Sci. 516, 182–191. https://doi.org/10.1016/j.jcis.2018.01.039

Kovalchuk, N.M., Nowak, E., Simmons, M.J.H., 2016. Effect of Soluble Surfactants on the Kinetics of Thinning of Liquid Bridges during Drops Formation and on Size of Satellite Droplets. Langmuir 32, 5069–5077. https://doi.org/10.1021/acs.langmuir.6b01467

Kovalchuk, N.M., Roumpea, E., Nowak, E., Chinaud, M., Angeli, P., Simmons, M.J.H., 2018b. Effect of surfactant on emulsification in microchannels. Chem. Eng. Sci. 176, 139–152. https://doi.org/10.1016/j.ces.2017.10.026

Kovalchuk, N.M., Sagisaka, M., Steponavicius, K., Vigolo, D., Simmons, M.J.H., 2019. Drop formation in microfluidic cross-junction: jetting to dripping to jetting transition.

Microfluid. Nanofluidics 23. https://doi.org/10.1007/s10404-019-2269-z

Leal, L.G., Stone, H.A., 1990. The effect of surfactant on drop deformation ans breakup. J. Fluid Mech. 220, 161–186.

Lei, L., Zhao, Y., Chen, W., Li, H., Wang, X., Zhang, J., 2021. Experimental studies of droplet formation process and length for liquid–liquid two-phase flows in a microchannel. Energies 14, 1–17. https://doi.org/10.3390/en14051341

Mastiani, M., Seo, S., Jimenez, S.M., Petrozzi, N., Kim, M.M., 2017. Flow regime mapping of aqueous two-phase system droplets in flow-focusing geometries. Colloids Surfaces A Physicochem. Eng. Asp. 531, 111–120. https://doi.org/10.1016/j.colsurfa.2017.07.083

Moiré, M., Peysson, Y., Herzhaft, B., Pannacci, N., Gallaire, F., Augello, L., Dalmazzone, C., Colin, A., 2017. Ultralow Interfacial Tension Measurement through Jetting/Dripping Transition. Langmuir 33, 2531–2540. https://doi.org/10.1021/acs.langmuir.7b00076

Murphy, S. V., Atala, A., 2014. 3D bioprinting of tissues and organs. Nat. Biotechnol. 32, 773–785. https://doi.org/10.1038/nbt.2958

Roth, E.A., Xu, T., Das, M., Gregory, C., Hickman, J.J., Boland, T., 2004. Inkjet printing for high-throughput cell patterning. Biomaterials 25, 3707–3715. https://doi.org/10.1016/j.biomaterials.2003.10.052

Roumpea, E., Kovalchuk, N.M., Chinaud, M., Nowak, E., Simmons, M.J.H., Angeli, P., 2019. Experimental studies on droplet formation in a flow-focusing microchannel in the presence of surfactants. Chem. Eng. Sci. 195, 507–518. https://doi.org/10.1016/j.ces.2018.09.049

Salim, A., Fourar, M., Pironon, J., Sausse, J., 2008. Oil-water two-phase flow in microchannels: FLow patterns and pressure drop measurements. Can. J. Chem. Eng. 86, 978–988. https://doi.org/10.1002/cjce.20108

Shahriari, A., Kim, M.M., Zamani, S., Phillip, N., Nasouri, B., Hidrovo, C.H., 2016. Flow

regime mapping of high inertial gas–liquid droplet microflows in flow-focusing geometries. Microfluid. Nanofluidics 20, 1–13. https://doi.org/10.1007/s10404-015-1671-4

Tice, J.D., Lyon, A.D., Ismagilov, R.F., 2004. Effects of viscosity on droplet formation and mixing in microfluidic channels. Anal. Chim. Acta 507, 73–77. https://doi.org/10.1016/j.aca.2003.11.024

Tostado, C.P., Xu, J.H., Du, A.W., Luo, G.S., 2012. Experimental study on dynamic interfacial tension with mixture of SDS-PEG as surfactants in a coflowing microfluidic device. Langmuir 28, 3120–3128. https://doi.org/10.1021/la204852w

Tsaoulidis, D., Dore, V., Angeli, P., Plechkova, N. V., Seddon, K.R., 2013. Flow patterns and pressure drop of ionic liquid-water two-phase flows in microchannels. Int. J. Multiph. Flow 54, 1–10. https://doi.org/10.1016/j.ijmultiphaseflow.2013.02.002

Utada, A.S., Fernandez-Nieves, A., Stone, H.A., Weitz, D.A., 2007. Dripping to jetting transitions in coflowing liquid streams. Phys. Rev. Lett. 99, 1–4. https://doi.org/10.1103/PhysRevLett.99.094502

Wang, K., Lu, Y.C., Xu, J.H., Luo, G.S., 2009. Determination of dynamic interfacial tension and its effect on droplet formation in the T-shaped microdispersion process. Langmuir 25, 2153–2158. https://doi.org/10.1021/la803049s

Wang, K., Zhang, L., Zhang, W., Luo, G., 2016. Mass-Transfer-Controlled Dynamic Interfacial Tension in Microfluidic Emulsification Processes. Langmuir 32, 3174–3185. https://doi.org/10.1021/acs.langmuir.6b00271

Wu, Z., Cao, Z., Sundén, B., 2017. Liquid-liquid flow patterns and slug hydrodynamics in square microchannels of cross-shaped junctions. Chem. Eng. Sci. 174, 56–66. https://doi.org/10.1016/j.ces.2017.08.032

Xu, J.H., Li, S.W., Tan, J., Luo, G.S., 2008. Correlations of droplet formation in T-junction

microfluidic devices: From squeezing to dripping. Microfluid. Nanofluidics 5, 711–717. https://doi.org/10.1007/s10404-008-0306-4

Yagodnitsyna, A.A., Kovalev, A. V., Bilsky, A. V., 2016. Flow patterns of immiscible liquid-liquid flow in a rectangular microchannel with T-junction. Chem. Eng. J. 303, 547–554. https://doi.org/10.1016/j.cej.2016.06.023

Zhao, C.X., Middelberg, A.P.J., 2011. Two-phase microfluidic flows. Chem. Eng. Sci. 66, 1394–1411. https://doi.org/10.1016/j.ces.2010.08.038

Zhao, Y., Chen, G., Yuan, Q., 2006. Liquid-liquid two-phase flow patterns in a rectangular microchannel. AIChE J. 52, 4052–4060. https://doi.org/https://doi.org/10.1002/aic.11029

Electronic Supplementary Information

Effect of surfactants on drop formation flow patterns in a flow-focusing microchannel

*Maria Kalli, Panagiota Angeli**

ThAMeS Multiphase, Department of Chemical Engineering, University College London, Torrington Place, London, WC1E 7JE, UK

*Author to whom correspondence should be addressed. Email: p.angeli@ucl.ac.uk

Langmuir-Szyszkowski adsorption isotherms

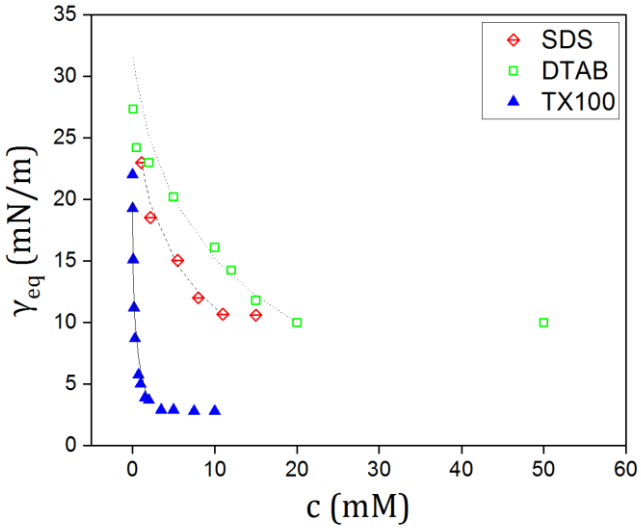

Figure S1: Equilibrium interfacial tension against concentration for SDS, DTAB and TX100 surfactants dissolved in 52% w/w glycerol solution